

# Morphology of Template-Grown Polyaniline Nanowires and Its Effect on the Electrochemical Capacitance of Nanowire Arrays

Yanyan Cao and Thomas E. Mallouk\*

Department of Chemistry, The Pennsylvania State University, University Park, Pennsylvania 16802

Received April 13, 2008. Revised Manuscript Received June 20, 2008

The morphology of polyaniline nanowires grown electrochemically in anodic aluminum oxide (AAO) templates is strongly influenced by the supporting electrolyte concentration, the potential of electropolymerization, the growth time, and the monomer concentration. Increasing the sulfuric acid concentration during growth induces a transition from solid nanowires with tubular ends to open nanowires. Current transient data for nanowire growth were interpreted quantitatively in terms of instantaneous and progressive nucleation and growth models, and this analysis was consistent with the observed concentration and potential dependence of nanowire vs nanotube growth. The electrochemical capacitance of nanowire arrays in AAO templates was shown to be related to the morphology of the nanowires. Specific capacitance values in the range of 700 F/g (measured at a charge/discharge rate of 5 A/g) were obtained for porous nanowires grown at 0.5 M aniline concentration at high overpotential in 1.5–2.0 M sulfuric acid solutions.

## Introduction

Intrinsically conducting polymers are useful materials in sensors, electroluminescent devices, polymer-based electronics, and organic photovoltaic cells, because they are electronically conducting or semiconducting while retaining the mechanical, processing, and cost advantages of polymers.<sup>1</sup> To exploit nanostructural effects in these devices, researchers have developed several methods for fabricating conducting polymers as thin films, nanospheres, nanowires, nanotubes, and core–shell structures.<sup>2,3</sup> Among these, the hard template method<sup>4–6</sup> is especially useful for making conducting nanowires and nanotubes of controllable dimensions. Resistors, diodes, and field-effect transistors based on conducting polymer nanowires have been demonstrated.<sup>7,8</sup> Fast electrochromic devices based on poly(3,4-ethylenedioxythiophene) (PEDOT) nanotubes have been described,<sup>9,10</sup> and the synthesis of polyaniline nanowires in AAO has also recently been reported.<sup>11</sup> We have recently studied conducting

polymer nanorods grown by the hard template method as sensors for solution-phase and gaseous analytes.<sup>12–14</sup>

Polyaniline is a particularly interesting conducting polymer because of its stability in air and in water, high conductivity in its oxidized/protonated form, acid–base properties, electrochromic behavior, and electrochemical capacitance.<sup>15</sup> Polyaniline has been used in sensors and biosensors,<sup>16–19</sup> solar cells,<sup>20</sup> batteries,<sup>21</sup> electrochromic devices,<sup>22</sup> and antistatic coatings.<sup>23</sup> Because of its high specific capacitance,<sup>24</sup> polyaniline is also one of the most promising materials for electrochemical supercapacitors.<sup>25,26</sup>

The porosity and internal structure of conducting polymer nanowires and nanotubes play a crucial role in their proper-

- 
- \* Corresponding author. E-mail: tom@chem.psu.edu.
- (1) Heeger, A. J. *Angew. Chem., Int. Ed.* **2001**, *40*, 2591.
  - (2) Jang, J. *Adv. Polym. Sci.* **2006**, *199*, 189.
  - (3) Li, G. F.; Martinez, C.; Semancik, S. *J. Am. Chem. Soc.* **2005**, *127*, 4903.
  - (4) Martin, C. R. *Acc. Chem. Res.* **1995**, *28*, 61.
  - (5) Martin, C. R.; Vandyke, L. S.; Cai, Z. H.; Liang, W. B. *J. Am. Chem. Soc.* **1990**, *112*, 8976.
  - (6) Penner, R. M.; Martin, C. R. *J. Electrochem. Soc.* **1986**, *133*, 2206.
  - (7) Hurst, S. J.; Payne, E. K.; Qin, L. D.; Mirkin, C. A. *Angew. Chem., Int. Ed.* **2006**, *45*, 2672.
  - (8) Park, S.; Chung, S. W.; Mirkin, C. A. *J. Am. Chem. Soc.* **2004**, *126*, 11772.
  - (9) Cho, S. I.; Choi, D. H.; Kim, S. H.; Lee, S. B. *Chem. Mater.* **2005**, *17*, 4564.
  - (10) Cho, S. I.; Kwon, W. J.; Choi, S. J.; Kim, P.; Park, S. A.; Kim, J.; Son, S. J.; Xiao, R.; Kim, S. H.; Lee, S. B. *Adv. Mater.* **2005**, *17*, 171.
  - (11) Zhao, G.; Li, H. *Microporous Mesoporous Mater.* **2007**, *48*, 19; **2008**, *110*, 590.

- (12) Cao, Y.; Kim, J.; Mayer, T. S.; Mallouk, T. E. *Polym. Prepr. (Am. Chem. Soc., Div. Polym. Chem.)* **2007**, *48*, 19.
- (13) Dan, Y.; Cao, Y.; Mallouk, T. E.; Johnson, A. T.; Evoy, S. *Sens. Actuators, B* **2007**, *125*, 55.
- (14) Hernandez, R. M.; Richter, L.; Semancik, S.; Stranick, S.; Mallouk, T. E. *Chem. Mater.* **2004**, *16*, 3431.
- (15) Huang, W. S.; Humphrey, B. D.; Macdiarmid, A. G. *J. Chem. Soc., Faraday Trans. 1* **1986**, *82*, 2385.
- (16) Wei, D.; Ivaska, A. *Chem. Anal.* **2006**, *51*, 839.
- (17) Nicolas-Debarnot, D.; Poncin-Epaillard, F. *Anal. Chim. Acta* **2003**, *475*, 1.
- (18) Huang, J.; Virji, S.; Weiller, B. H.; Kaner, R. B. *Chem.—Eur. J.* **2004**, *10*, 1315.
- (19) Virji, S.; Huang, J. X.; Kaner, R. B.; Weiller, B. H. *Nano Lett.* **2004**, *4*, 491.
- (20) Tan, S. X.; Zhai, J.; Wan, M. X.; Jiang, L.; Zhu, D. B. *Synth. Met.* **2003**, *137*, 1511.
- (21) Cheng, F. Y.; Tang, W.; Li, C. S.; Chen, J.; Liu, H. K.; Shen, P. W.; Dou, S. X. *Chem.—Eur. J.* **2006**, *12*, 3082.
- (22) DeLongchamp, D. M.; Hammond, P. T. *ACS Symp. Ser.* **2005**, *888*, 18.
- (23) Maziarz, E. P.; Lorenz, S. A.; White, T. P.; Wood, T. D. *J. Am. Soc. Mass Spectrom.* **2000**, *11*, 659.
- (24) Lota, K.; Khomenko, V.; Frackowiak, E. *J. Phys. Chem. Solids* **2004**, *65*, 295.
- (25) Belanger, D.; Ren, X. M.; Davey, J.; Uribe, F.; Gottesfeld, S. *J. Electrochem. Soc.* **2000**, *147*, 2923.
- (26) Takei, T.; Kobayashi, Y.; Hata, H.; Yonesaki, Y.; Kumada, N.; Kinomura, N.; Mallouk, T. E. *J. Am. Chem. Soc.* **2006**, *128*, 16634.

ties and device performance.<sup>10,27–30</sup> However, the means of controlling their morphology without the use of templates are so far rather limited. Huang and Kaner developed rapid-mixing and interfacial polymerization methods to make polyaniline nanofibers chemically.<sup>31–33</sup> Liu and co-workers devised a three-step electrochemical route to polyaniline nanowires.<sup>34</sup> However, nanotubes, nanofibers, and nanowires made by these methods are either interconnected or nonuniform. In this paper, we describe a systematic study of the electrochemical growth of polyaniline from aqueous H<sub>2</sub>SO<sub>4</sub> solutions in anodic aluminum oxide (AAO) membranes, and the effect of different parameters on the morphology of the resulting nanowires. The galvanostatic charge–discharge method was used to measure the electrochemical capacitance of arrays of polyaniline nanowires, which correlates well with their morphology. Current transient data for nanowire growth can be interpreted quantitatively in terms of instantaneous and progressive nucleation and growth models, and this analysis is consistent with the observed concentration and potential dependence of nanowire versus nanotube growth.

### Experimental Section

Aniline, sulfuric acid, gold plating solution (Orotemp 24), and gold etchant (GE-8148) were purchased from Aldrich Chemical Co., EMD, Technic Inc., and Transene Company Inc., respectively. AAO membranes (Anodisc 25 with 0.2 μm pore diameter) were purchased from Whatman. Dialysis tubing with 12 000–14 000 molecular weight cutoff was obtained from Spectrum Chemical and Laboratory Products.

Light microscopy was carried out with an Olympus BX60 M reflected-light microscope equipped with an Olympus U-CMAN-2 camera (Olympus, Japan). Transmission electron microscopy (TEM) images were obtained with a JEOL 1200 EXII at 80 kV accelerating voltage. Electrochemical experiments were performed using either a BAS 100B or a EG&G/Princeton Applied Research model 363 potentiostat/galvanostat in a one-compartment, three-electrode cell at room temperature. A BAS LG-50 galvanostat was used to perform the constant current charge–discharge characterization. The reference electrode was a saturated calomel electrode (SCE). All potential values are reported versus the SCE. A Pt coil was used as the counter electrode.

A layer of gold about 110 nm thick was deposited onto the branched side of the AAO membranes using a BOC Edwards FL400/Auto306 thermal evaporator. This gold film was used as the working electrode contact for further electroplating of gold and polymerization of aniline in the pores. A gold layer a few micrometers thick was electroplated galvanostatically at 0.65 mA/cm<sup>2</sup> current density before the aniline polymerization step. Polymerization was done at constant potential in aqueous solutions of aniline and sulfuric acid under varying conditions of concentration. TEM samples were prepared by dissolving the gold back of the

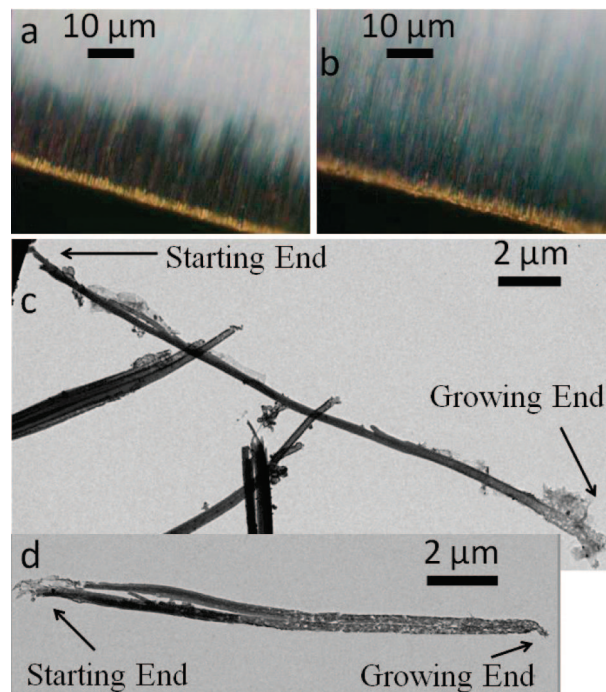


**Figure 1.** Optical microscope and TEM images of polyaniline nanowires grown in (a, c) 0.25 and (b, d) 1.5 M H<sub>2</sub>SO<sub>4</sub> solutions. Other conditions (monomer concentration = 0.1 M, polymerization potential = 900 mV, charge passed = 5 C) were the same for both.

membrane in the gold etchant followed by dissolving the membrane in 5 M H<sub>2</sub>SO<sub>4</sub> at 40 °C for 20 h. The nanowires were then purified by dialysis against Millipore nanopure water or methanol for 2 days.

The mass of the polyaniline nanowire array was measured by using the following procedure. The AAO membrane was rinsed thoroughly with water, dried under flowing nitrogen and stored in a vacuum desiccator for several hours. The weight was then measured on a Sartorius BP211D balance to an accuracy of 0.01 mg. After polyaniline deposition, the membrane was rinsed, dried and weighed in the same way. Because the alumina membranes slowly dissolve in the H<sub>2</sub>SO<sub>4</sub>-based polymerization solution, the weight of the polyaniline nanowires has to be compensated by the alumina weight loss. The polymerization solution was therefore collected after the reaction, and the aluminum concentration in the solution was measured on a Leeman Laboratories PS3000UV inductively coupled plasma spectrophotometer and converted to alumina weight loss of the membrane.

### Results and Discussion

**Effect of Electrolyte Concentration.** We observed that H<sub>2</sub>SO<sub>4</sub> concentration strongly affects the morphology of the resulting polyaniline nanowires. Figure 1 shows optical microscope images in cross-section of alumina membranes containing the nanowires, and TEM images of typical wires released from the membranes. In the optical images, the gold-colored band is the evaporated and electroplated gold that functions as the working electrode contact. The dark band above the gold is the polymer contained in the parallel cylindrical pores. Nanowires grown in 0.25 M H<sub>2</sub>SO<sub>4</sub> solution are typically dense. The TEM image (Figure 1c) of such a wire shows a predominantly solid cylinder with a tubular morphology and thinning tube walls near the growth

- (27) Gupta, V.; Miura, N. *Electrochem. Solid-State Lett.* **2005**, *8*, A630.  
 (28) Zhou, H. H.; Chen, H.; Luo, S. L.; Lu, G. W.; Wei, W. Z.; Kuang, Y. F. *J. Solid State Electrochem.* **2005**, *9*, 574.  
 (29) Zou, X. H.; Zhang, S.; Shi, M. H.; Kong, J. L. *J. Solid State Electrochem.* **2007**, *11*, 317.  
 (30) Xiao, R.; Il Cho, S.; Liu, R.; Lee, S. B. *J. Am. Chem. Soc.* **2007**, *129*, 4483.  
 (31) Huang, J. X.; Kaner, R. B. *J. Am. Chem. Soc.* **2004**, *126*, 851.  
 (32) Huang, J. X.; Kaner, R. B. *Angew. Chem., Int. Ed.* **2004**, *43*, 5817.  
 (33) Huang, J. X.; Kaner, R. B. *Chem. Commun.* **2006**, *4*, 367.  
 (34) Liang, L.; Liu, J.; Windisch, C. F.; Exarhos, G. J.; Lin, Y. H. *Angew. Chem., Int. Ed.* **2002**, *41*, 3665.

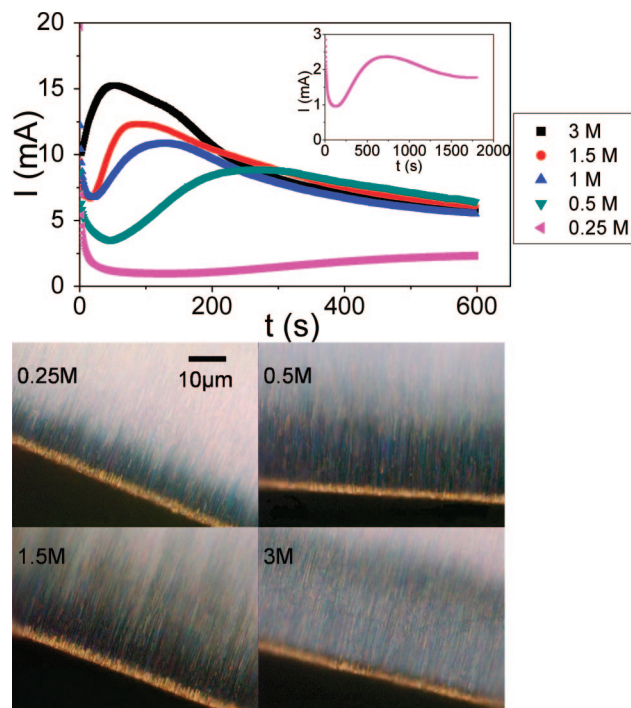


**Figure 2.** Current transients (upper) and optical images (lower) of aniline polymerization at different  $\text{H}_2\text{SO}_4$  concentrations. The monomer concentration was 0.1 M and the polymerization potential was 900 mV. The inset in the upper graph shows the  $I-t$  transient for aniline polymerization in 0.25 M  $\text{H}_2\text{SO}_4$  on a longer time scale.

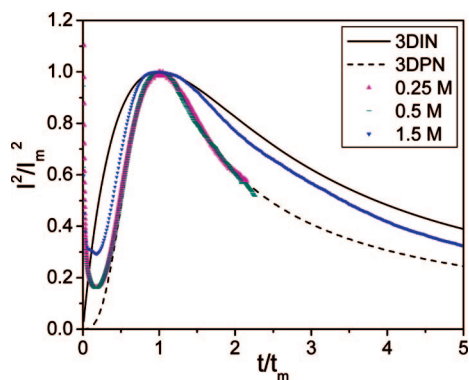


**Figure 3.** Dimensionless plots of  $I-t$  behavior, comparing data from Figure 2 with theoretical curves for three-dimensional progressive and instantaneous nucleation under diffusion control.

end. In contrast, the nanowire (Figure 1d) grown in 1.5 M  $\text{H}_2\text{SO}_4$  solution appears tubular (from the light contrast in the center of the cylinder) for most of the length of the wire.

Conducting polymer morphology depends on nucleation and growth processes.<sup>35</sup> Therefore in order to understand the morphology observed under different synthetic conditions, it is necessary to study the nucleation and growth mechanism. Current transients of polymerization are commonly used to probe the nucleation and growth mechanisms of conducting polymers. Figure 2 shows current transients from a series of experiments in which the  $\text{H}_2\text{SO}_4$  concentration was varied from 0.25 to 3 M. The inset shows the current transient at 0.25 M  $\text{H}_2\text{SO}_4$  concentration on a longer time scale. All the  $I-t$  curves follow the same trend. There is an

initial current drop, which is typical of polyaniline electropolymerization. It has been attributed in different studies to charging current, oxidative electroadsorption of monomers, and substrate passivation.<sup>35–37</sup> Following the initial current drop, the current rises slowly to a maximum value before gradually falling again.

The current maximum can be analyzed by comparing the  $I-t$  data with theoretical plots for different modes of polyaniline nucleation and growth. The theoretical  $I-t$  characteristics for three-dimensional instantaneous nucleation (3DIN) and three-dimensional progressive nucleation (3DPN) under diffusion control are given by eqs 1 and 2, respectively<sup>37–39</sup>

$$\frac{I}{I_m} = \frac{1.9542}{t/t_m} \{1 - \exp[-1.2564(t/t_m)]\}^2 \quad (1)$$

$$\frac{I}{I_m} = \frac{1.2254}{t/t_m} \{1 - \exp[-2.3367(t/t_m)^2]\}^2 \quad (2)$$

Figure 3 compares dimensionless current–time plots, obtained from the experimental data in Figure 2 with theoretical curves for progressive and instantaneous 3D nucleation processes under the diffusion control. At low  $\text{H}_2\text{SO}_4$  concentration, very good agreement between the experimental data and the theoretical plot for progressive nucleation under diffusion control is obtained. At higher  $\text{H}_2\text{SO}_4$  concentrations, the experimental data fall in the region between progressive and instantaneous nucleation, which are two extreme cases of the nanowire growth mechanism.

The 3D nucleation model suggests that in the early stage of polymerization, the current increases as a result of the increase of the number of nuclei and their size. The growth rate is controlled by hemispherical diffusion to the nuclei. At a certain point, the growth rate reaches saturation as hemispherical diffusion gives way to linear diffusion. The current then decreases as the monomer concentration near the electrode decreases.

Referring again to Figure 2, the current maximum shifts to a shorter time and higher current as the  $\text{H}_2\text{SO}_4$  concentration increases. This can be explained by a faster diffusion rate of monomers to the electrode at higher  $\text{H}_2\text{SO}_4$  concentration. The increase in diffusion coefficient with increasing electrolyte concentration has been observed in other systems<sup>40,41</sup> and is possibly due to the modulation of the hydrodynamic radius of the diffusing species as the ionic strength changes.<sup>42</sup>

Another effect of increased  $\text{H}_2\text{SO}_4$  concentration is the increased rate of hydrolysis of polyaniline under anodic conditions,<sup>43</sup> which is an important reason for the increased porosity of the nanowires. There is thus a tradeoff between the porosity and the stability of the polyaniline nanowires.

(36) Sazou, D.; Kourouzidou, M.; Pavlidou, E. *Electrochim. Acta* **2007**, *52*, 4385.

(37) Scharifker, B.; Hills, G. *Electrochim. Acta* **1983**, *28*, 879.

(38) Hwang, B. J.; Santhanam, R.; Wu, C. R.; Tsai, Y. W. *J. Solid State Electrochem.* **2001**, *5*, 280.

(39) Mandic, Z.; Duic, L.; Kovacic, F. *Electrochim. Acta* **1997**, *42*, 1389.

(40) Kariuki, S.; Dewald, H. D. *Electroanalysis* **1997**, *9*, 231.

(41) Stromova, E.; Pak, V. *Russ. J. Appl. Chem.* **2006**, *79*, 1709.

(42) Sasaki, S. *Colloid Polym. Sci.* **1984**, *262*, 406.

(43) Vivier, V.; Cachet-Vivier, C.; Regis, A.; Sagon, G.; Nedelec, J. Y.; Yu, L. T. *J. Solid State Electrochem.* **2002**, *6*, 522.

(35) Cordova, R.; Delvalle, M. A.; Arratia, A.; Gomez, H.; Schrebler, R. *J. Electroanal. Chem.* **1994**, *377*, 75.

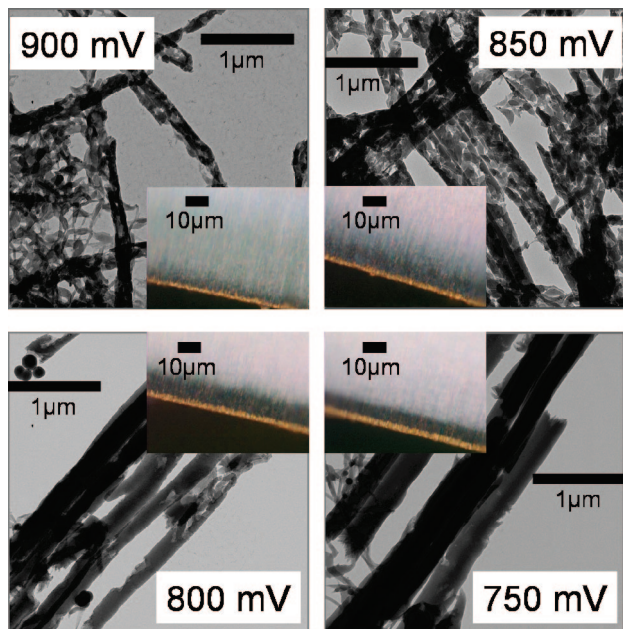


**Figure 4.** TEM and optical images of polyaniline nanowires synthesized at different potentials.

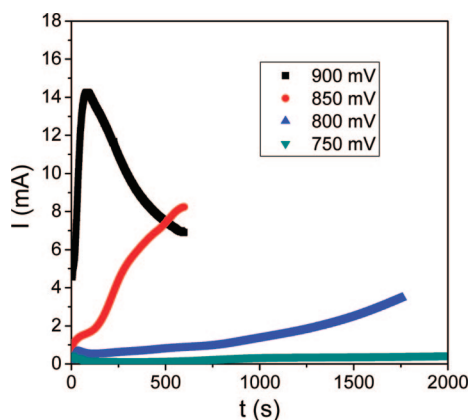


**Figure 5.** Current transients of polyaniline synthesized at different potentials.

At 0.1 M aniline concentration, when the  $\text{H}_2\text{SO}_4$  concentration is over 2M, the synthesized nanowires are not stable and lose their electrochemical activity after several charge–discharge cycles in the potential window of 0–0.7 V versus SCE.

**Effect of Polymerization Potential.** Figure 4 shows the transition from porous to dense nanowires as the potential of polymerization is made less anodic. In these experiments, the monomer concentration was kept at 0.1 M and the  $\text{H}_2\text{SO}_4$  concentration was kept at 2M, i.e., under similar conditions that gave a mixture of progressive and instantaneous 3D nucleation at a potential of 900 mV in Figure 3.

To understand the mechanism of nucleation and growth, we again recorded current transients during polymerization (Figure 5). At 900 mV, as expected, the  $I-t$  curve follows the diffusion-limited 3D nucleation and growth model. However, at potentials lower than 800 mV, a completely different behavior was observed. The current increases exponentially with a shoulder at an early stage of the reaction. The exponential current increase is consistent with one-

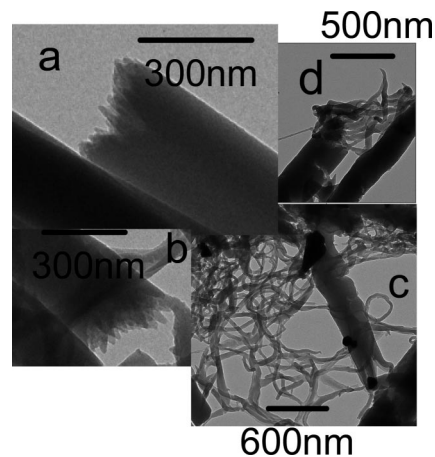


**Figure 6.** TEM images of samples synthesized under 1D chain branching growth. (a, b) Saw-tooth ends of nanowires. (c, d) Some loose nanofibers in the nanowire suspension. The sample in a and b was grown in a solution of 0.1 M aniline and 2 M  $\text{H}_2\text{SO}_4$  at 750 mV. The sample in c and d was grown in a solution of 0.2 M aniline and 2 M  $\text{H}_2\text{SO}_4$  at 800 mV.

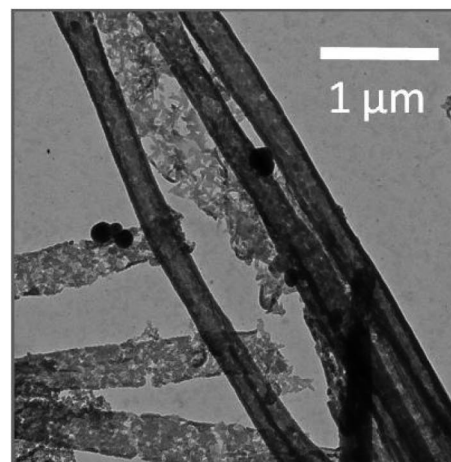
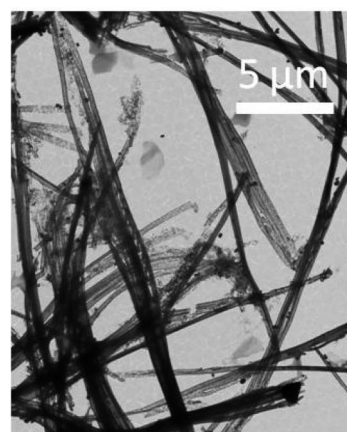


**Figure 7.** Tubular shape of the growth end of the nanowires grown in a solution of 0.1 M aniline and 0.5 M  $\text{H}_2\text{SO}_4$  at 900 mV.

dimensional chain branching.<sup>39,44</sup> However, no specific morphology has been clearly connected to this kind of growth in the literature. Therefore, we studied the morphology of nanowires grown under 1D chain branching conditions. The body of the nanowire always appears dense under the optical

(44) Bade, K.; Tsakova, V.; Schultze, J. W. *Electrochim. Acta* **1992**, *37*, 2255.

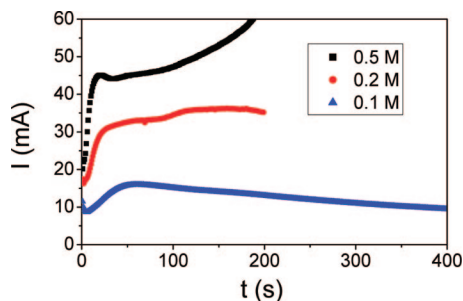


**Figure 8.** Effect of aniline concentration on the current transients with  $\text{H}_2\text{SO}_4$  concentration controlled at 2 M.

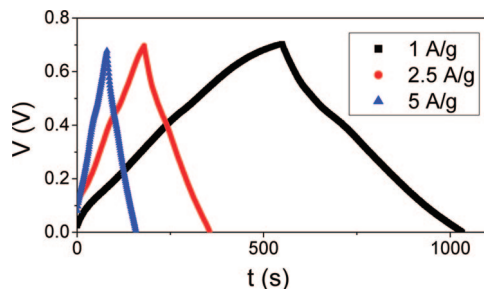


**Figure 9.** Galvanostatic charge-discharge curves of a polyaniline nanowire array synthesized in a solution of 0.1 M aniline and 1.5 M  $\text{H}_2\text{SO}_4$  at 900 mV.

microscope. What is interesting is that many of the nanowires have saw-tooth ends, which suggests that the nanowires are actually bundles of interconnected nanofibers that are 30–80 nm in diameter (images a and b in Figure 6). This observation is consistent with the hypothesis of Kaner<sup>33</sup> that polyaniline possesses an intrinsic morphology of nanofibers. Indeed, we observed some free nanofibers (images c and d in Figure 6) in the nanowire suspension.

In comparison, 3D nucleation under diffusion control usually gives nanowires with a tubular end of decreasing wall thickness at low  $\text{H}_2\text{SO}_4$  concentration. In this case, no nanofibers are found in the suspensions. The top end of the tube becomes very thin and in some cases breaks off as thin flakes. A typical example is shown in Figure 7a. The total length of these nanowires is about 20  $\mu\text{m}$ . More than 75% of the growth end of the wire is tubular with decreasing wall thickness toward the end. Figure 7b illustrates the tubular morphology and the different wall thickness at different points along the tube. As the initially tubular nanowires grow with time, both the length and the proportion of the dense part increase. In contrast, when the  $\text{H}_2\text{SO}_4$  concentration is high, the nanowires remain porous throughout their growth.

**Effect of Monomer Concentration.** The applicability of the diffusion-controlled mechanism should also depend on

the monomer concentration, because Fick's first law states that the diffusion flux is proportional to the concentration gradient.<sup>45</sup> Indeed, we observed a transition in the current transient behavior at high monomer concentration, as shown in Figure 8. At 0.1 M aniline concentration, the  $I-t$  transient has the shape expected for 3D nucleation and growth under diffusion control. At 0.5 M, there is a current maximum followed by continuous current increase, reminiscent of the behavior observed at lower overpotential in Figure 5. Under these conditions, the growth appears to follow a combined 3D and 1D mechanism. TEM images showed that the nanowires become denser with increasing monomer concentration, consistent with this hypothesis.

**Electrochemical Capacitance.** The galvanostatic charge-discharge method is a reliable way to characterize the electrochemical capacitance of materials under controlled current conditions. This measurement is relevant to the use of conducting polymers in different morphologies as components of supercapacitors.<sup>27,46–49</sup> Figure 9 shows the charge-discharge curves of a typical polyaniline nanowire array at three different charge-discharge rates. The measurements were done in 1 M sulfuric acid with the polyaniline nanowire arrays inside the AAO membranes.

The specific capacitance ( $C_s$ ) was evaluated via the equation  $C_s = I/(m \, dV/dt)$ , where  $I$  is the discharge current,  $m$  is the total mass of the polyaniline nanowires in the array, and  $dV/dt$  can be obtained from the slope of the discharge curve. The results on several different samples are shown in Table 1. To understand the effect of the nanowire array configuration, we also synthesized polyaniline films on gold-covered glass slides for comparison. The specific capacitance of nanowire arrays is slightly higher than that of films made under the same conditions. This is exemplified by sample 1 and sample 2. The specific capacitance of the array structure (sample 2) is about 20% more than that of the film (sample 1). This is easy to understand because the nanowire array structure improves the accessibility of electrolytes as a result of the partial etching of AAO membrane in the electrolyte. The specific capacitance of the arrays can be further increased by complete removal of the AAO membrane (data not shown).

Comparing sample 2 and sample 3, one can see the effect of the electrolyte concentration on specific capacitance. As discussed above, higher  $\text{H}_2\text{SO}_4$  concentration induces a more open morphology. Consequently, sample 3, which was made in 2 M  $\text{H}_2\text{SO}_4$ , has higher specific capacitance than sample 2, which was made in 0.5 M  $\text{H}_2\text{SO}_4$ . A similar trend was seen in sample 4 and sample 5. When the  $\text{H}_2\text{SO}_4$  concentra-

**Table 1.** Comparison of Polyaniline Samples Synthesized under Different Conditions

sample no.	polymerization conditions	mass of polyaniline (mg)	$C_s$ at a discharging rate of 1 A/g (F/g)	$C_s$ at a discharging rate of 2.5 A/g (F/g)	$C_s$ at a discharging rate of 5 A/g (F/g)
1 (film)	0.5 M aniline, 0.5 M $\text{H}_2\text{SO}_4$ , 900 mV	2.4	440	430	400
2 (array)	0.5 M aniline, 0.5 M $\text{H}_2\text{SO}_4$ , 900 mV	3.3	520	500	480
3 (array)	0.5 M aniline, 2 M $\text{H}_2\text{SO}_4$ , 900 mV	1.6	760	730	710
4 (array)	0.1 M aniline, 0.25 M $\text{H}_2\text{SO}_4$ , 900 mV	2.0	550	520	480
5 (array)	0.1 M aniline, 1.5 M $\text{H}_2\text{SO}_4$ , 900 mV	0.77	780	700	610
6 (array)	0.2 M aniline, 2 M $\text{H}_2\text{SO}_4$ , 800 mV	1.6	410	370	340
7 (array)	0.2 M aniline, 2 M $\text{H}_2\text{SO}_4$ , 900 mV	1.4	540	460	430

tion increased from 0.25 M to 1.5M, the specific capacitance of the array also increased.

The effect of polymerization potential on specific capacitance is illustrated by sample 6 and sample 7. Sample 6 was made at 800 mV and has a dense morphology. Sample 7 was synthesized at 900 mV and shows some porosity under TEM. This leads to higher specific capacitance in sample 7.

The monomer concentration effect is somewhat surprising. Comparing sample 3 and sample 7, the higher monomer concentration in sample 3 led to a sample of slightly denser morphology than sample 7. However, the specific capacitance of sample 3 is actually higher. This can be attributed to the poor integrity of sample 7 caused by hydrolysis, which was confirmed by the observation of broken polyaniline pieces in TEM images. Monomer concentration is another important factor in determining the degree of hydrolysis because of the competitive reaction between aniline and water with the polaronic hydrolysis precursor.<sup>50</sup> Thus, sample 3, which was made in a solution of high aniline concentration, has good sample integrity even at high H<sub>2</sub>SO<sub>4</sub> concentrations.

Sample 3 has a specific capacitance of 710 F/g at a discharging rate of 5A/g. To the best of our knowledge, this is close to the highest reported value of polyaniline capacitance, approximately 768 F/g, at similar discharging rates.<sup>27,49</sup> Further optimization may be possible by fine-tuning of the synthetic conditions or by using other strategies. For example, it has been demonstrated that conducting polymer composite nanowires with metal oxides of high specific capacitance exhibit improved supercapacitor performance.<sup>48</sup> Selective removal of the inorganic phase in conducting polymer composite nanowires is an effective way to introduce extra porosity into the nanowires.<sup>51</sup> Despite the porous nature of these samples, preliminary tests showed good electrochemical stability. A sample prepared from a solution of 0.1 M aniline and 0.5 M H<sub>2</sub>SO<sub>4</sub> at 900 mV vs SCE (similar to that shown in Figure 7) showed only a 7% decrease in the slope of the discharge curve after 410 galvanostatic charge–discharge cycles from 0 to 600 mV at 4 mA.

Energy density and power density are also used as figures of merit for capacitors. It has been reported<sup>25</sup> that a type I capacitor based on two symmetric polyaniline film electrodes has an energy density of 2.7 Wh/kg at the power density of 1 kW/kg. Taking into account that the equivalent circuit of a type I capacitor is two identical capacitors in series, the energy density and power density of a symmetric type I capacitor can be estimated as  $1/4E_s$  and  $1/4P_s$ , respectively, where  $E_s$  and  $P_s$  are the energy density and power density values measured in a three-electrode system. The factor of 1/4 comes from the fact that the series capacitance and mass

are, respectively, half and double that of a single capacitor. The following equations are used to calculate  $E_s$  and  $P_s$  from the charge–discharge measurements in a three-electrode system

$$E_s = E/m \quad (3)$$

$$E = I \int V dt \quad (4)$$

where the integral  $\int V dt$  is obtained from the area under the galvanostatic discharge curve

$$P_s = P/m, \quad (5)$$

and

$$P = dE/dt \quad (6)$$

Using sample 4 in Table 1 as an example, a type I capacitor would have energy densities of approximately 10, 9.3, and 7.7 Wh/kg at power densities of 0.7, 1.9, and 3.5 kW/kg, respectively. We can conclude that at similar power density, the energy density of the polyaniline nanowire arrays is higher than that of reported polyaniline films<sup>25</sup> and is similar to that of poly(3,4-ethylenedioxythiophene) nanotubes in AAO membranes.<sup>52</sup> However, the thickness of commercial alumina membranes is limited to about 60  $\mu\text{m}$ . Thus, the amount of polyaniline in an electrode prepared in this manner is limited to a few milligrams per  $\text{cm}^2$ . Thus, the total power and energy are very limited. From applications point of view, it remains to be seen if polyaniline nanowire arrays with similar porosity can be grown on higher surface area electrode structures, either by growing hard templates conformally on the electrode or by using soft template methods.

## Conclusions

The electrochemical synthesis of polyaniline nanowires in aqueous H<sub>2</sub>SO<sub>4</sub> solutions was investigated. Increasing the H<sub>2</sub>SO<sub>4</sub> concentration during growth induces a transition from solid nanowires with tubular ends to open nanowires. The nanowire morphology correlates with nucleation and growth mechanisms deduced from current–time transients. At high anodic potential (900 mV), the current transient data fit a 3D diffusion-controlled nucleation and growth model. Depending on the H<sub>2</sub>SO<sub>4</sub> concentration, the nanowires can exhibit a porous morphology or have a tubular growth end with decreasing wall thickness toward the tip. At lower anodic potential, the  $I-t$  curves fit a 1D chain branching model. The resulting nanowires have a dense morphology and appear to consist of interconnected small fibers. The electrochemical capacitance of polyaniline nanowire arrays was characterized as a function of growth conditions. In general, open morphology and better sample integrity increase the specific capacitance.

**Acknowledgment.** This work was supported by the National Science Foundation under NIRT Grant ECS-0303981. We thank Henry Gong of the Penn State Materials Characterization Laboratory for the inductively coupled plasma emission spectrometric analysis of aluminum concentrations. The TEM images were taken at the Electron Microscopy Facility of the Huck Institutes of the Life Sciences at Penn State.

CM801028A

(45) Bard, A. J.; Faulkner, L. R., *Electrochemical Methods: Fundamentals and Applications*, 2nd ed.; John Wiley and Sons: New York, 2001.

(46) Winter, M.; Brodd, R. J. *Chem. Rev.* **2004**, *104*, 4245.

(47) Conway, B. E.; Birss, V.; Wojtowicz, J. *J. Power Sources* **1997**, *66*, 1.

(48) Liu, R.; Lee, S. B. *J. Am. Chem. Soc.* **2008**, *130*, 2942.

(49) Wang, Y. G.; Li, H. Q.; Xia, Y. Y. *Adv. Mater.* **2006**, *18*, 2619.

(50) Cui, C. Q.; Ong, L. H.; Tan, T. C.; Lee, J. Y. *Electrochim. Acta* **1993**, *38*, 1395.

(51) Meenach, S. A.; Burdick, J.; Kunwar, A.; Wang, J. *Small* **2007**, *3*, 239.

(52) Liu, R.; Cho, S. II.; Lee, S. B. *Nanotechnology* **2008**, *19*, 215710.